Investigations concerning wing-body interference for compressible flow

Georg Wichmann
Deutsche Forschungsanstalt für Luft- und Raumfahrt e.V. (DLR)
Institute of Design Aerodynamics
Postfach 3267, D-38022 Braunschweig, Germany

Abstract

Numerical results concerning wing-body interference for compressible flow obtained by the use of an Euler method are presented. Beside the presentation of the basic mechanism of the mutual influence of wing and body there are pointed out the numerical results which had been obtained using simple principle models to determine the body effects and the Mach number effects on pressure and lift distributions of the configuration. A detailed analysis of the total lift behaviour of wing and body confirm the basic results.

1. Introduction

Because of economic reasons the design of transport aircraft requires a reasonable knowledge of flight mechanics behaviour as soon as possible during the design process. To fullfil this demand aerodynamics has to provide the corresponding data. In this context a detailed knowledge of the mutual influence of the flow around the components of the aircraft (interference) is of great importance, because often its influence on the total behaviour of the aircraft is of the same order of magnitude as the contributions of the single parts of the aircraft alone[1].

The aerodynamic interaction between wing and body - wing body interference - had been very early a research object in fluid dynamics [2, 3]. So body lift could be identified as a force induced directly by the wing circulation and it had been shown that the velocity field of the body crossflow for its part induces an additional wing lift [4].

In incompressible flow there exist a lot of experimental as well as theoretical investigations, working out the basic interference effects [5]. By the use of modern methods, like Euler and Navier-Stokes codes, e.g. [6, 7], up to now isolated solutions for special configurations with high accuracy had been obtained, which however do not allow any statements about the physical background of the interaction between wing and body. A detailed knowledge about the interference effects on pressure and lift distributions of wing and body in the compressible flow regime however is of high importance especially with regard to an optimum design of transport aircraft at high subsonic Mach numbers. For this reason at the Institute for Design Aerodynamics at DLR systematic parameter studies had been performed using an Euler method, with the aim to close the lack of knowledge considered before. The present paper is limited to the presentation of the results obtained during the investigations with variation of body radius and the free stream Mach number. The complete version of the topic considered is published in [8] and in extracts in [9].

2. Numerical method

The computational grids required for the application of the Euler method are based on a C-H topology [10]. In streamwise direction they show a C structure, in spanwise direction a H structure. After providing a starting grid a smooth and non-overlapping 3D mesh had been generated using an elliptical grid generator with source term control in wall proximity [11]. The applied topology, the spatial point distribution as well as the point density on the surface of a realistic wing-body configuration indicates **fig.1**. Especially the important region of the wing-body junction and the wing itself show very fine resolution.

A basic description of the Euler method used named CEVCATS is given in [12]. The basic equations as well as the solution algorithm are presented in detail in [13]. The computational method is based on the equations of motion for three-dimensional compressible inviscid flow in integral form. Its numerical solution is based on a discretization separately done in spatial and time direction. The spatial discretization is done using the Finite Volume method, where the discrete equations form a system of first order differential equations. It will be solved using an explicit five step Runge-Kutta time step method with several tools for convergence acceleration [12].

3. Results

3.1 Fundamentals of wing-body interference

Considering a wing-body configuration the wing is situated in the induced velocity field of the body and vice versa. The interactions of these perturbation fields lead to interference effects, which especially influence the pressure and lift distributions of wing and body. Lifting wings generate velocity fields, which are characterized by induced upwash velocities in front of the wing and downwash behind. An estimation of the influence of these velocity fields on the flow around the body leads to the following statements (see also [4] and [14]):

- The wing-influenced total body lift is only a quantity induced by the wing.

- Approximately it has the same value as the lift of the part of the wing covered by the body.

Fig.2 schematically shows the flow field of an body with incidence in streamwise direction. One can see that the non influenced body does not generate any resulting force but only a pitching moment. The total body lift is zero, if the body is closed at nose and tail. The flow around the body can be divided into a displacement flow parallel to the body axis and a crossflow normal to the body axis. In comparison to the crossflow the displacement flow generates perturbation velocities which are so small that its influence can be neglected [14].

In **Fig.3** schematically is shown the velocity field normal to body axis induced by an infinite body with a circular cross section. It is identical to the velocity field of the flow around a circular cylinder.

The normal velocities resulting from this crossflow can be interpreted as an additional distribution of angle of incidence. Along the spanwise direction in mid wing position ($y > R$) then results:

$$\frac{\Delta\alpha(y)}{\alpha_\infty} = \frac{\alpha(y) - \alpha_\infty}{\alpha_\infty} = \frac{R^2}{y^2} . \qquad (1)$$

With this additional distribution of angle of incidence as body influence on the wing flow the application of the Kutta-Joukowsky theorem on a flat plate wing with chord c and c_o as chord at the wing root yields an additional wing lift caused by the body (spanwise integration with $\Gamma_\infty = \pi \cdot c_o \cdot V_\infty \cdot \alpha_\infty$ and $K = 2 \cdot \rho_\infty \cdot V_\infty \cdot \Gamma_\infty$)

$$\Delta L_W = K \int_{y=R}^{s} \frac{c(y)}{c_o} \cdot \frac{R^2}{y^2} dy \qquad (2)$$

and a corresponding total wing lift

$$L_W = K \int_{y=R}^{s} \frac{c(y)}{c_o} \cdot \left[1 - \frac{\alpha_i(y)}{\alpha_\infty} + \frac{R^2}{y^2} \right] dy . \qquad (3)$$

The determination of the total lift of a wing-body configuration is done like in [4], where the calculation of the lift acting on the body is performed by the reflection of the wing vortex system at the body surface (**fig.4**). Far behind the wing in the Trefftz plane the influence of the bound vortices disappears and only the influence of the free vortices remain. In a cross section normal to the body axis the flow can be regarded as two-dimensional. The application of the mirror principle of the free vortices at the body surface than automatically fulfills the tangential flow condition on the body surface. With a given wing circulation from this procedure can result statements about the body lift, but not about its distribution along the body axis.

Finally for a wing-body configuration with a wing, which is not influenced by a body (zero body incidence, wing decalage), results the body lift

$$L_B = K \int_{y=R}^{s} \frac{c(y)}{c_o} \cdot \left(1 - \frac{\alpha_i(y)}{\alpha_\infty} \right) \cdot \frac{R^2}{y^2} dy \qquad (4)$$

and corresponding the total lift of the configuration

$$L_{(W+B)} = K \int_{y=R}^{s} \frac{c(y)}{c_o} \left(1 - \frac{\alpha_i(y)}{\alpha_\infty} \right) \left(1 + \frac{R^2}{y^2} \right) dy . \qquad (5)$$

The comparison of eq.(2) and eq.(4) as well as eq.(3) and eq.(5) respectively shows that they are identical if the distribution of the induced angle of incidence $\alpha_i(y)$ is neglected. This is allowed if high aspect ratio wings are considered where is $|\alpha_i(y)/\alpha_\infty| \ll 1$. Thus follows for high aspect ratio wings with given distribution of circulation that the additional wing lift ΔL_W caused by the body incidence approximately is equal to the body lift L_B caused by the wing with zero incidence of the body:

$$\Delta L_{W \text{ body incidence}} \approx L_{B \text{ zero body incidence}} \qquad (6)$$

and similarly that the total wing lift L_W, which is influenced by the body with incidence, approximately has the same value as the total lift $L_{(W+B)}$ of a corresponding wing-body configuration with wing decalage (zero incidence of the body):

$$L_{W \text{ body incidence}} \approx L_{(W+B) \text{ zero body incidence}} . \qquad (7)$$

Furthermore from this can be derived a simple relationship for the ratio generated from the body lift and the total lift of the considered wing-body configuration if the wing circulation is assumed to be constant:

$$\frac{L_B}{L_{(W+B)}} = \frac{\eta_R}{1 + \eta_R} . \qquad (8)$$

Here $\eta_R = R/s$ is the relative body radius. Corresponding to the general statements initially made about the body lift, eq.(8) shows that the body takes over the lift which would have been generated by the part of wing covered by the body.

3.2 The investigated wing-body arrangements

The systematic investigations to determine wing-body interference effects have been performed using simple principle models. There are based on symmetric wing-body arrangements, which allow a clear separation of the different interference effects of wing and body. The fundamental configuration is shown in **fig.5**.

A survey of the investigated configurations is given in **fig.6**. The investigations to determine the body influence have been performed using two different types of configuration, each with three different bodies (case KI, KII, KIII). Type A is characterized by the feature that with variation of body radius the half span s of the configuration is kept constant, while for configuration type B the half span of the wing s_W is unchanged, i.e. the half span s varies with variation of the body radius.

In both cases, type A and B, there will occur the same physical effects, so in the frame of this paper it will be sufficient to investigate only one type, namely type A. But it should be mentioned that investigating type B an additional effect must be taken into consideration which arises from the effective change of the aspect ratio of the configuration with variation of the body radius.

The wing body flow can be divided into the two classical components of the problems of wing theory i.e. displacement and lift problem. The lift problem will be divided in two cases: The case of body incidence and wing decalage (**fig.7**). In the case of body incidence wing and body have the same angle of attack, while in the case of wing decalage the wing has an angle of attack (decalage) ε relative to the body. The body itself has zero incidence.

3.3 Variation of body radius

For the determination of the body displacement effect on the wing pressure distribution a comparison between a simple wing-body model with a rectangular wing geometry and the corresponding two rectangular wings alone has been performed, where the symmetry planes of these wings have been placed in the symmetry plane of the body (continuous wing 1) or in the plane of the wing-body junction (wing 2) respectively (**fig.8**). The pressure distributions in a selected plane near the body show that the wing suction pressure is reduced by the presence of the body, i.e. the body acts decelerating on the wing flow. This effect is due to the three-dimensional shape of the wing-body junction, which in this case leads to diverging streamlines in the near body region. Furthermore, this fact means that the near body wing pressure distributions are decisively dependent on the shape of the wing-body junction and less dependent on the pure displacement effect of the finite body.

The pressure distribution of a swept wing is essentially influenced by a sweep effect acting in the symmetry region of the wing, called „desweep effect" of a swept wing, because it leads to a desweep of isobars in this region [15]. This effect also will appear in the wing-body junction region of a wing-body configuration. Regarding the displacement problem the „desweep effect" is leading to flow decelerations in the front part of the wing and to accelerations in the rear part respectively. In the case of the lift problem this effect results in lower loads in the front part of wing and in higher loads in the rear part, respectively.

In the following will be described the interference effects which occur for swept models (configuration type A with leading edge sweep angle φ = 36,7° (fig.5)). **Fig.9** and **fig.10** show the results for the case with displacement flow alone ($\alpha = 0°$; $\varepsilon = 0°$) when the body radius varies.

In fig.9 are plotted pressure distributions in three spanwise wing sections for the considered bodies as well as the corresponding pressure distribution for the limiting case R = 0, which is the wing alone configuration. Its symmetry plane is identical to the symmetry plane of the configuration with body. The pressure distributions are essentially influenced by effects described above, namely flow deceleration due to body presence and desweep effect (see also the comparison between configuration KIIA and the wing alone in fig.10). The effects are increasing with increasing body radius, in spanwise direction the body influence decreases.

The corresponding results for the lift case with body incidence at $M_\infty = 0.8$ and $\alpha = 4°$ are shown in **fig.11** and **fig.12**. In the lift case with body incidence ($\varepsilon = 0°$) the wing is situated in a body induced upwash velocity field, which acts like an additional distribution of angle of incidence. Indeed its influence is first visible in section 3 of the presented pressure distributions. Here the pressure distributions show a clear downstream shock displacement. In section 1 the desweep effect and the deceleration effect predominate as is also shown in fig.12, where the pressure distributions of the configuration KIIA and the wing alone are compared separately. The spanwise lift distributions are plotted in the upper part of fig.11. Clearly be to seen are the lift losses in the near body region of the wing, increasing with increasing body radius. Further one can see that this influence is effective along a certain distance in the spanwise direction, amplified by the effect of the local zero body incidence due to flow distortion into the direction of wing chord. After decrease of this effect the wing lift is increasing in spanwise direction with increasing body radius due to the additional angle of incidence. The resulting lift values then are higher than the value of the wing alone. Also clearly to be seen is the decrease of the local lift value in the body region, reflecting the distribution of the finite wing circulation.

The results of the investigations with wing decalage for the configuration type A are presented in **fig.13** and **fig.14**. This arrangement is of high value for practical designs because it corresponds to a transport aircraft configuration at cruise condition with a body in horizontal position (α = 0°), while the wing has an incidence relative to the body (decalage). Opposed to the case with body incidence the incoming flow is not deflected in the body region but is nearly undisturbed in the streamwise direction from what follows a local reduction of angle of attack in the near body region of the wing. The results show that this zero incidence effect is the main influence parameter with respect to the wing lift distribution.

Fig. 13 shows the body influence on the lift and pressure

distributions. The main difference compared to the case with body incidence is that the body due to its zero incidence reduces the lift level generally and induces no additional upwash velocities at the wing position and consequently no additional wing lift. As shown in fig.14 also the desweep effects near the body are effective.

Fig.15 shows the total lift behaviour of the configuration type A in dependence on the body radius proportional for wing and body. One can see that with body incidence opposed to the wing decalage case, where results a lift reduction due to the body zero incidence with increasing body radius, the total lift values are nearly the same as for the wing alone. The comparison between the curve of wing lift contribution with body incidence (left part of the figure) and the total lift curve (wing and body of the wing decalage case (right part)) shows that the corresponding lift values are approximately the same (see also eq.(7)):

$$L_{(W+B)\text{ wing decalage}} \approx L_{W\text{ body incidence}} \cdot \qquad (9)$$

This statement together with a precise analysis of spanwise distribution of the mutual induced lift forces of wing and body lead to the following relations(**fig.16**):

$$L_{B\text{ wing decalage}}(\varepsilon) \approx \Delta L_{W\text{ body incidence}}(\alpha) \, . \qquad (10)$$

This result means that the body lift induced by a wing, which is twisted by a decalage angle ε, is approximately the same as the additional wing lift induced by the body with $\alpha = \varepsilon$ incidence. As shown above, this result is valid for a configuration with an infinite cylindrical body and a high aspect ratio wing in mid wing position where the influence of the induced angle of attack can be neglected. It leads to the result that the deviations of the lift curves in the middle part of fig.15 can definitely be reduced to the influence of the induced angle of attack. The higher lift level for the case with body incidence shows, due to the higher value of the induced angle of attack, a comparatively higher lift loss than in the case with wing decalage.

The next figure (**fig.17**) shows the c_L - α curves for the three investigated wing-body configurations KIA, KIIA and KIIIA as well as for wing A alone. The lift slope is approximately the same for all configurations. Also plotted is the lift curve for the case with wing decalage. It shows the same slope but a certain displacement to a smaller zero angle of attack.

3.4 Influence of Mach number

The total lift portions of wing and body are shown in **fig.18** in dependence on the Mach number for the configuration KIIA. The nomenclature corresponds to the quantities in fig.16. The lift increases nonlinearly with increasing Mach number, whereas the different lift portions all increase uniformly. The ratio generated from the body lift and the total lift of the configuration is plotted in **fig.19** dependent on Mach number. Also given is the curve of the lift ratio for the case of consltant wing circulation, the lower limit of the lift ratio (see eq. (8)). In this case the wing possesses the maximum lift, so that the relative body portion reaches a minimum value. In [8] is demonstrated that this lift ratio is directly dependent on the distribution of the wing circulation. It increases the more the higher the circulation deviates from the corresponding constant distribution along span. In the considered case (fig.19) without the portion of the body alone - body lift is alone wing induced (eq.(4)) - a constant distribution results, corresponding to a constant shape of wing circulation $\gamma(\eta)$ when Mach number changes (**fig.20**). This statement is also valid, if the boundary layer displacement thickness is taken into consideration when the wing flow is calculated (γ_0: circulation at wing root). With regard to the body lift alone a small decrease of the lift ratio results when the Mach number increases, because the wing lift portion due to local supersonic fields increases nonlinearly faster with increasing Mach number than the lift of the body alone.

3.5 Comparison with measurements

Fig.21 presents a comparison with measurements, which had been performed with the principle model in the year 1970 in the Transonic Wind Tunnel (TWG) at DLR Göttingen [16]. The figure shows with the configuration KIIA as example that the case with body incidence as well as the case with wing decalage are in good agreement with the measured values, where the calculations had been done under consideration of the boundary layer displacement thickness ([8], [17]).

4. Summary

In the present paper results of numerical investigations concerning wing-body interference for compressible flow are presented, which had been obtained using an Euler method.The computational meshes necessary had been obtained using an elliptical grid generation method.

The fundamental investigations resulted in the following:

- The interference effects are based on the mutual induced velocity fields of wing and body respectively.
- The body lift is a quantity only induced by the wing (wing circulation).
- The additional wing lift caused by the body with incidence (additional angle of attack) is approximately the same as the body lift induced by the wing when the body has zero incidence. This further means that the wing lift of a configuration where the wing is influenced by the body with incidence is approximately the same as the total lift of a configuration with zero incidence of the body.

The numerical investigations showed that pressure and lift distributions are influenced by

- flow deceleration in the near body region of the wing (3D wing-body junction)
- desweep effect of the finite wing in the wing-body junction region
- body incidence (additional angle of attack)
- change of effective aspect ratio when body radius varies and wing half span is constant
- twist effect of the body (zero incidence) in the case of wing decalage and consequently a decrease of total lift level.

With variation of Mach number it can be stated that

- the ratio generated from the body lift and the total lift of the configuration (wing and body) is approximately constant.

Comparisons with wind tunnel measurements show fairly good agreements between the calculated and measured values.

5. References

[1] Haines, A.B.:
Aerodynamic Interference - A General Overview
AGARD Report No.712: Special Course on Subsonic/Transonic Aerodynamic Interference for Aircraft. (1983), S.9/1-9/52.

[2] Lennertz, J.:
Beitrag zur theoretischen Behandlung des gegenseitigen Einflußes von Tragfläche und Rumpf.
ZAMM 7 (1927), S. 249 - 276.

[3] Vandrey, F.:
Zur theoretischen Behandlung des gegenseitigen Einflußes von Tragläche und Rumpf.
Luftf.-Forschg. 14 (1937), S. 347 - 355.

[4] Schlichting, H.; Truckenbrodt, E.:
Aerodynamik des Flugzeuges.
Bd. II, 2. Aufl., Berlin/Heidelberg/New York: Springer Verlag, 1969.

[5] Körner, H.:
Berechnung der potential-theoretischen Strömung um Flügel-Rumpf-Kombinationen und Vergleich mit Messungen (Dissertation; ausführliche Fassung).
DFVLR-Bericht Nr. 0679 (1971).

[6] Agrawal, S.; Lowie, R.B.; Creasman, S.F.:
An evaluation of Euler solvers for transonic flowfield computations on wing-fuselage geometries.
AIAA-Paper 90-3015 (1990).

[7] Fujii, K.; Obayashi, S.:
Navier-Stokes simulations of transonic flows over a wing-fuselage combination.
AIAA-Paper 86-1831 (1986).

[8] Wichmann, G.:
Untersuchungen zur Flügel-Rumpf-Interferenz durch Anwendung eines Eulerverfahrens für kompressible Strömungen.
ZLR-Forschungsbericht 93-06, Dissertation TU Braunschweig, (1993).

[9] Wichmann, G.:
Untersuchungen zur Flügel-Rumpf-Interferenz im kompressiblen Geschwindigkeitsbeeich.
DGLR Jahrbuch 1993 I (1993), DGLR 93-03-84, S. 233 - 245.

[10] Leicher, S.; Fritz, W.; Grashof, J.; Longo, J.:
Mesh Generation Strategies for CFD on Complex Configurations.
Lecture Notes in Physics, Vol. 170, Eight International Conference on Numerical methods in Fluid Dynamics.
Berlin/Heidelberg: Springer Verlag, 1982, S. 329 - 334.

[11] Sonar, Th.:
Grid Generation Using Elliptic Partial Differential Equations.
DFVLR-FB 89-15 (1989).

[12] Radespiel, R.; Rossow, C.-C.; Swanson, R.C.:
Efficient Cell-Vertex Multigrid Scheme for the Three-Dimensional Navier-Stokes Equations.
AIAA-Journal, Vol. 28, No.8, (1990), S. 1464 - 1472.

[13] Rossow, C.-C.:
Berechnung von Strömungsfeldern durch Lösung der Euler-Gleichungen mit einer erweiterten Finite-Volumen Diskretisierungsmethode.
DLR-FB 89-38 (1989).

[14] Multhopp, H.:
Zur Aerodynamik des Flugzeugrumpfes.
Luftf.-Forschg. 18, (1942), S. 52 - 66.

[15] Küchemann, D.; Weber, J.:
On the Chordwise Lift Distribution at the Centre of Swept Wings.
Aeron. Quarterly 2 (1950/51), S. 146 - 155.

[16] Schneider, W.:
Druckverteilungsmessungen an Pfeilflügel-Rumpf-Anordnungen bei hohen Unterschall-Machzahlen.
Teil II: Flügel mit dickem Rumpf.
AVA Bericht 70A 40 (1970).

[17] Wichmann, G.:
Ein Verfahren zur Berechnung der Umströmung von Flügel-Rumpf-Konfigurationen unter Berücksichtigung der Tragflügelgrenzschicht.
7. DGLR-Fachsymposium „Strömungen mit Ablösung", 7. - 9. Nov. 1990, Aachen, DGLR-Bericht 90-06, (1990), S. 56 - 60.

6. Figures

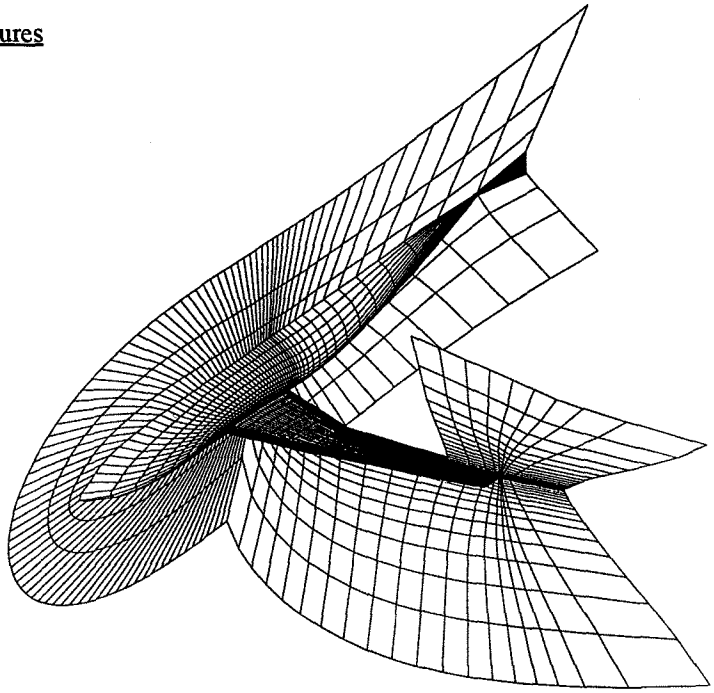

Fig. 1 Surface grid and mesh structure

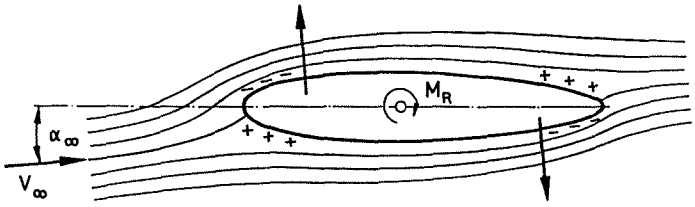

Fig. 2 Inviscid flow around a body with incidence

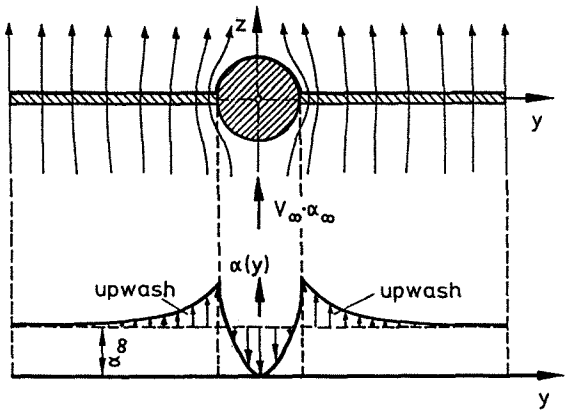

Fig. 3 Flow in a plane normal to the body axis of a wing-body configuration and schematical distribution of angle of attack along wing span

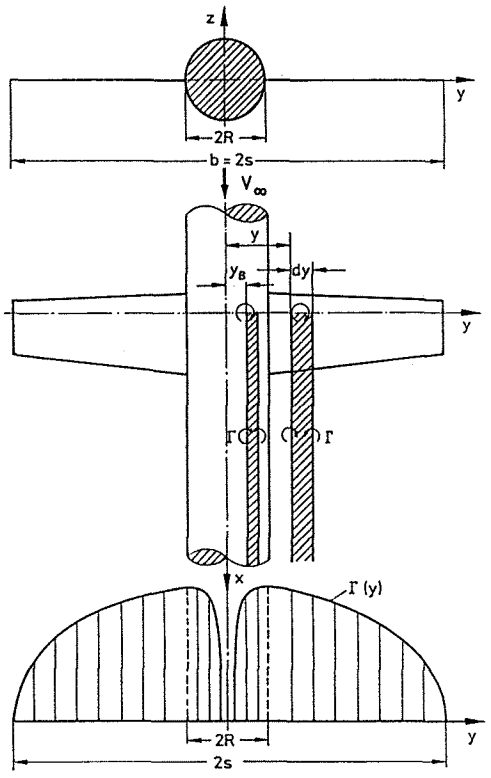

Fig. 4 planform and vortex system of a wing-body arrangement for the determination of the total lift

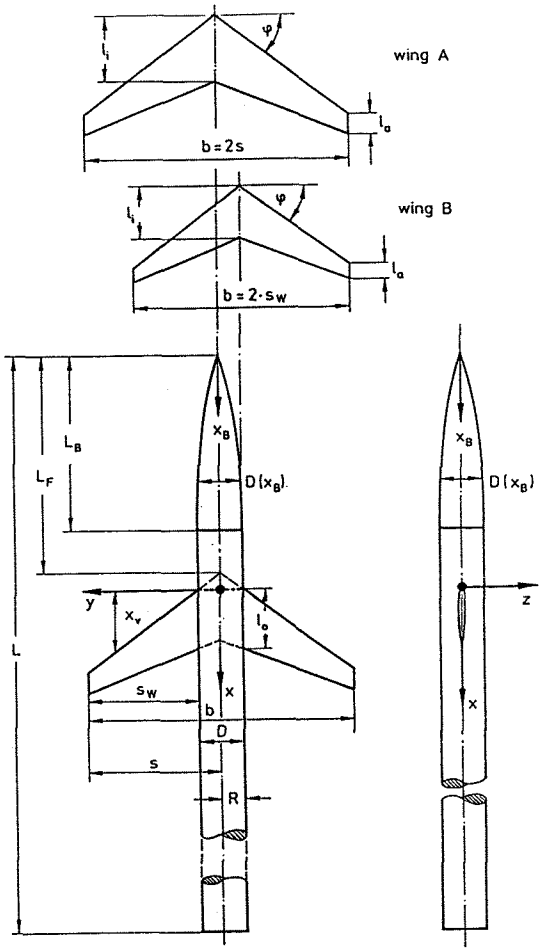

Fig. 5 Geometry of the basic model

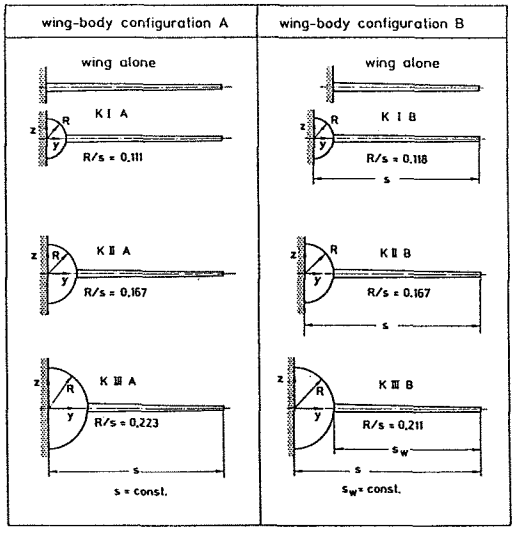

Fig. 6 Investigated configurations of the principle models

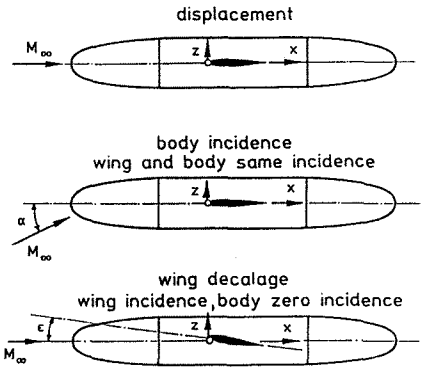

Fig. 7 Classification of the flow cases for wing-body configurations after displacement and lift problem

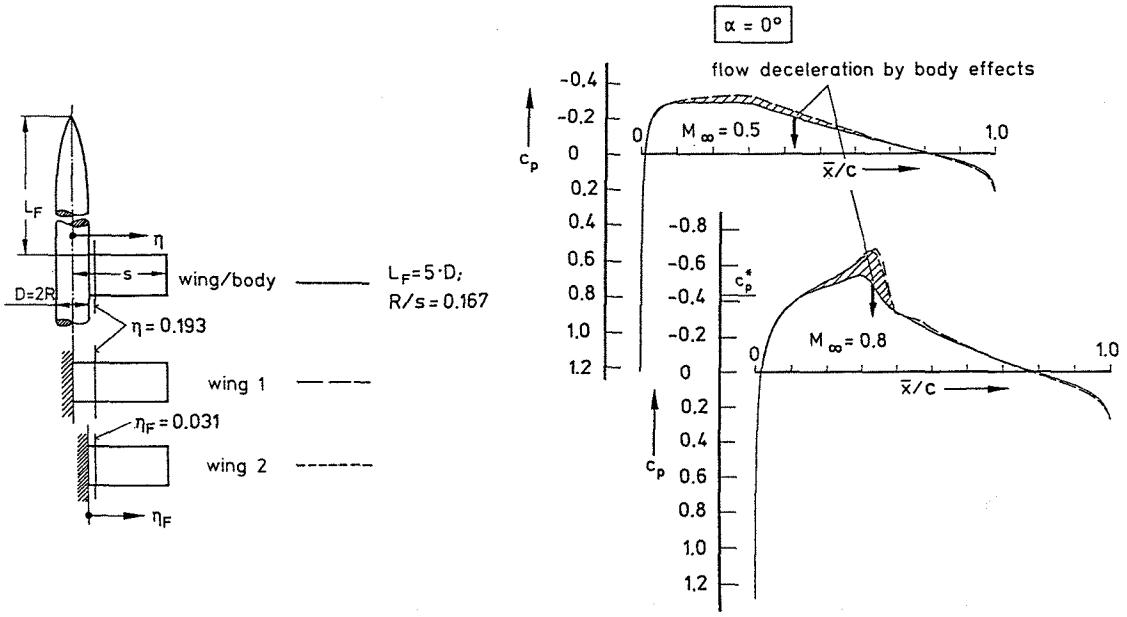

Fig. 8 Body influence on the pressure distribution of a rectangular wing at $M_\infty = 0.5$ and $M_\infty = 0.8$ ($\alpha = 0°$)

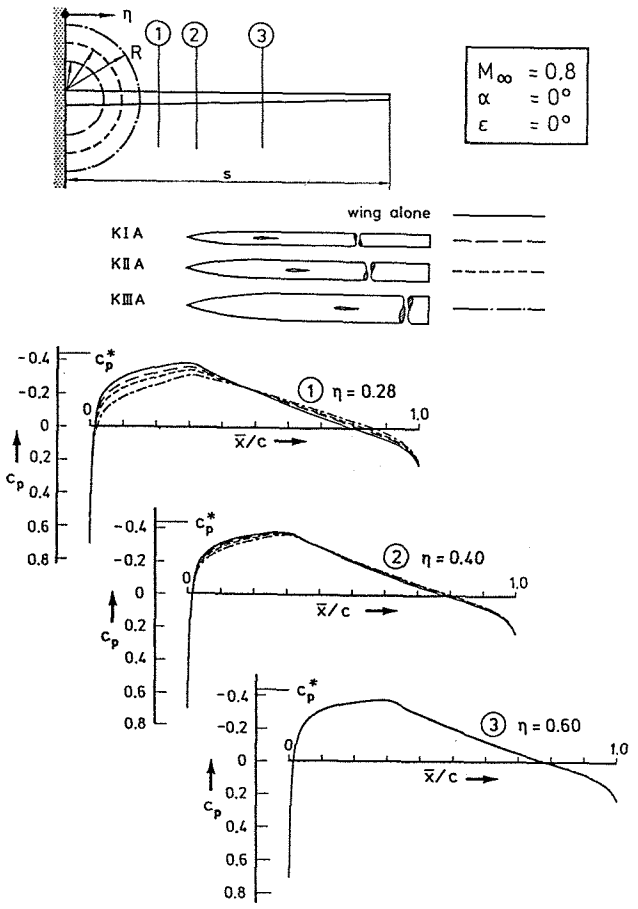

Fig. 9 Variation of body radius:
Pressure distribution at $M_\infty = 0.8$
(displacement case)

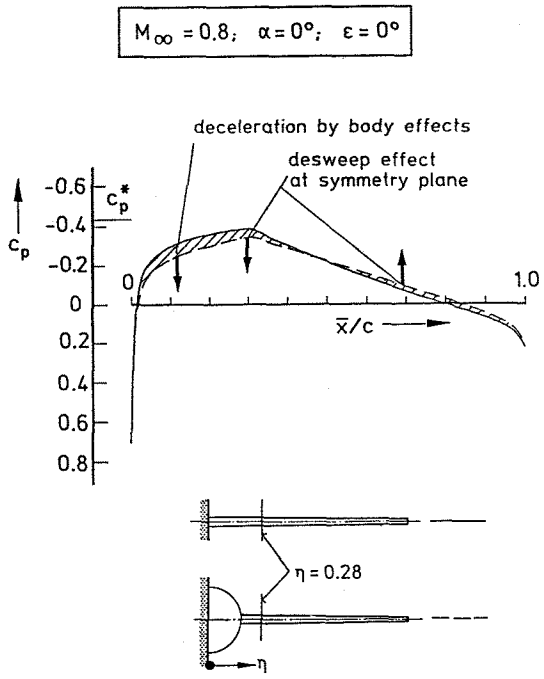

Fig. 10 Comparison of pressure distribution:
configuration KIIA and wing A alone at
$M_\infty = 0.8$ (displacement case)

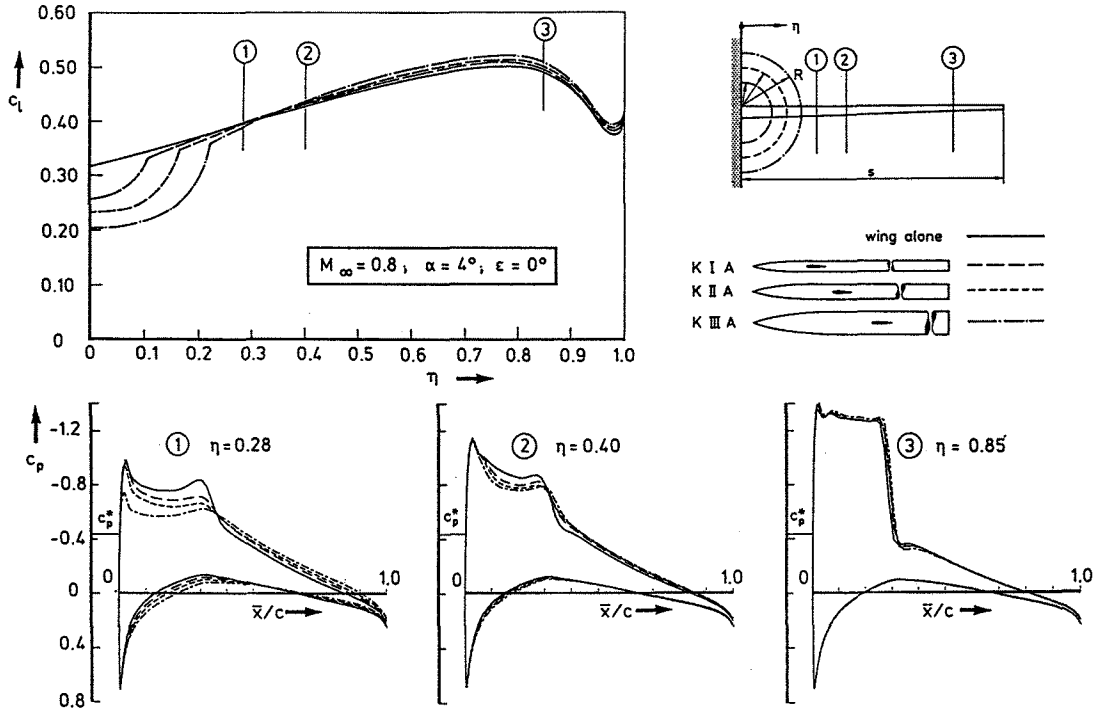

Fig. 11 Variation of body radius: Pressure and lift distributions at $M_\infty = 0.8$ (lift case, body with incidence)

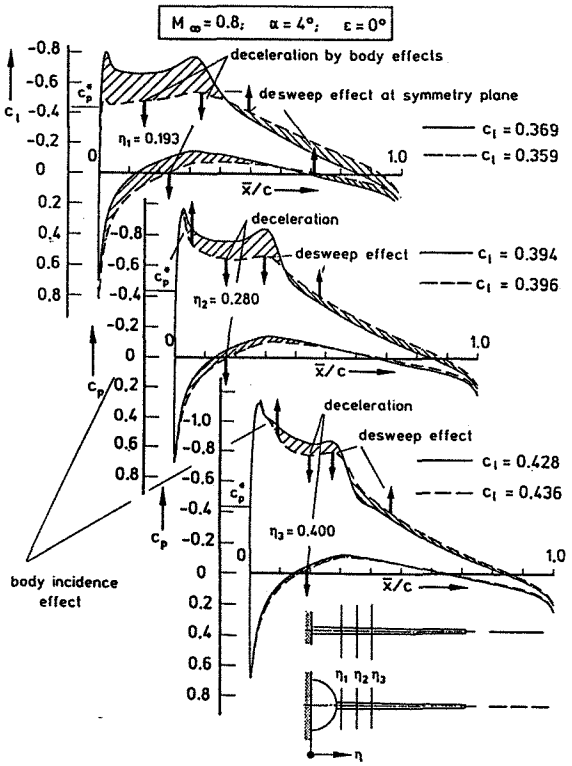

Fig. 12 Comparison of pressure distribution configuration KIIA and wing A alone at $M_\infty = 0.8$ (lift case, body with incidence)

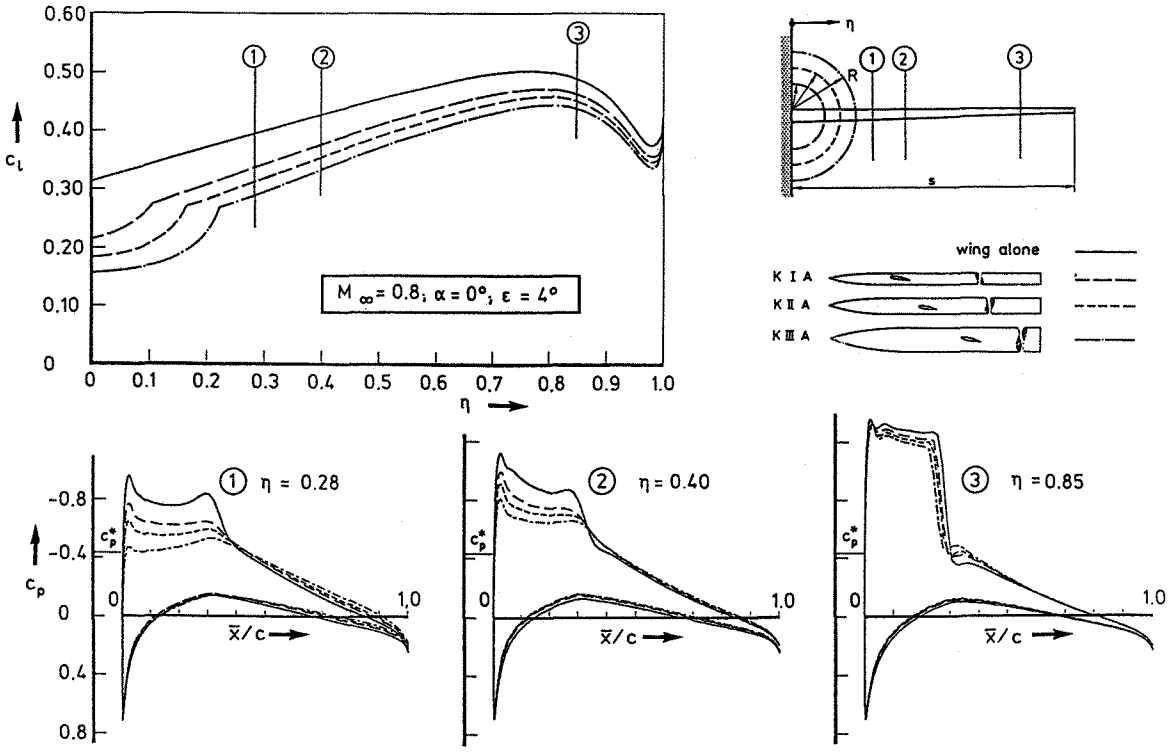

Fig. 13 Variation of body radius: Pressure and lift distributions at $M_\infty = 0.8$ (wing decalage)

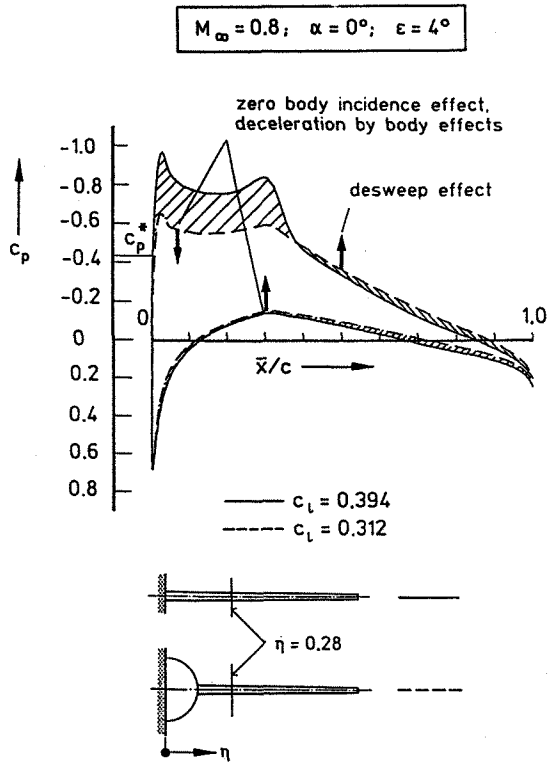

Fig. 14 Comparison of pressure distribution: configuration KIIA and wing A alone at $M_\infty = 0.8$ (wing decalage)

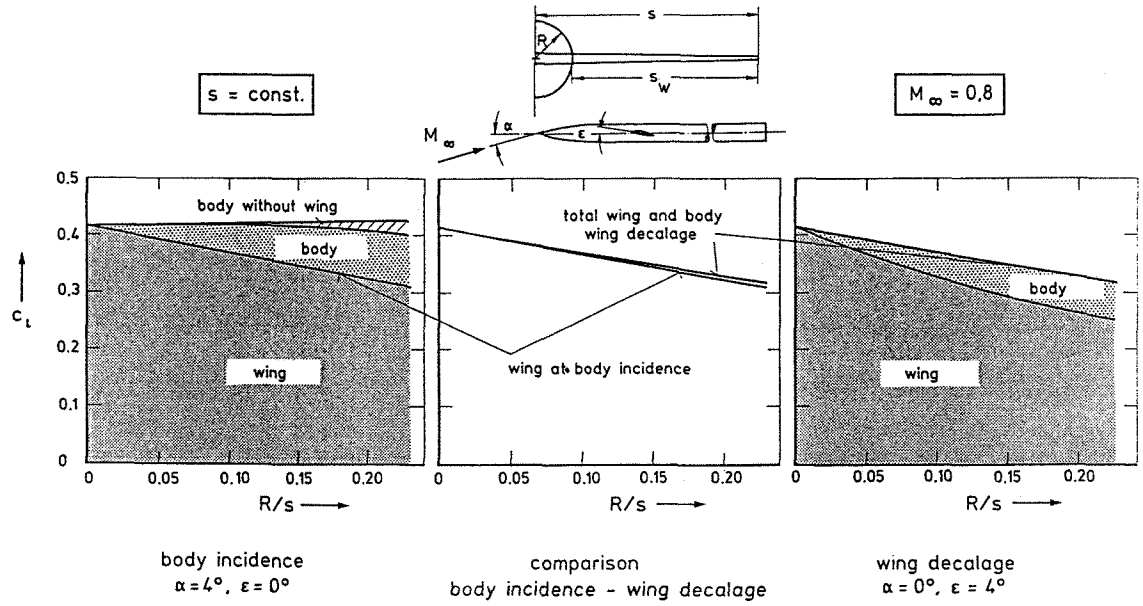

Fig. 15 Total lift of the principle model in dependence of body radius at $M_\infty = 0.8$

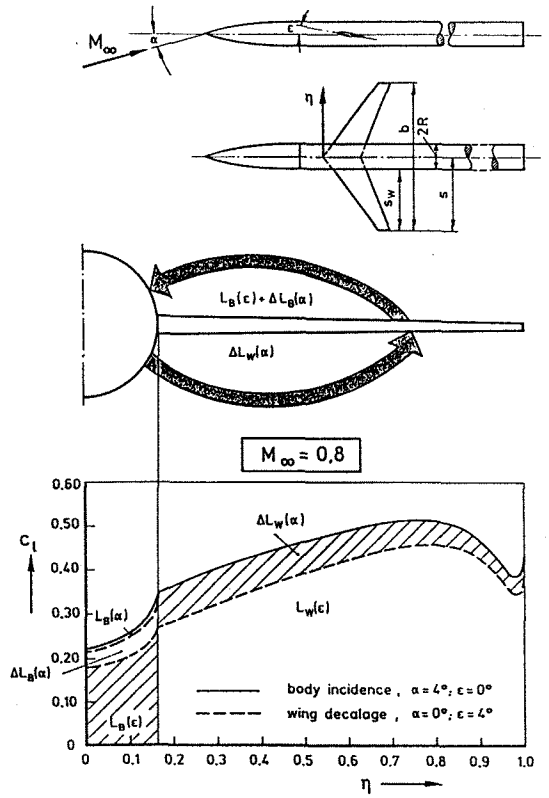

Fig. 16 Mutual induced lift forces of wing and body of the principle model at $M_\infty = 0.8$

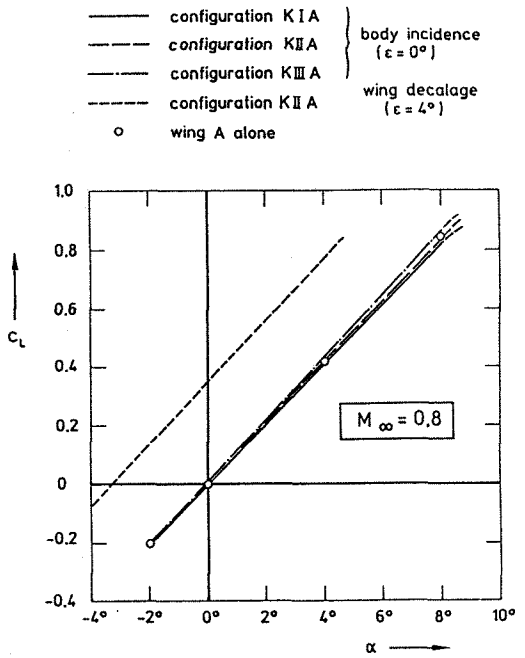

Fig. 17 Total lift of the principle model in dependence of angle of attack at $M_\infty = 0.8$

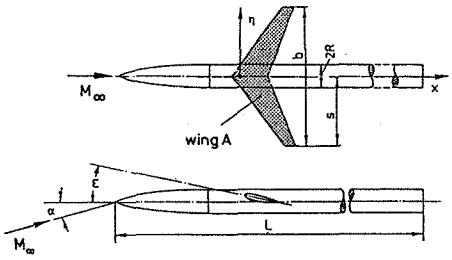

configuration K II A

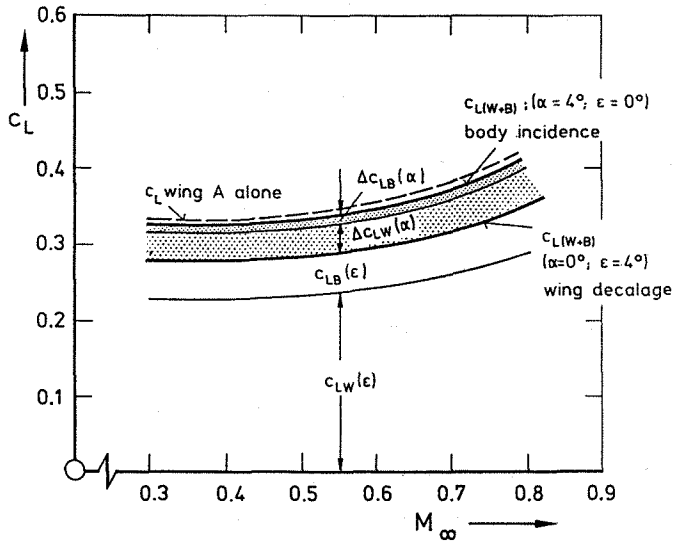

Fig. 18 Total lift of the principle model in dependence of Mach number, lift contributions of wing and body (see also fig.16)

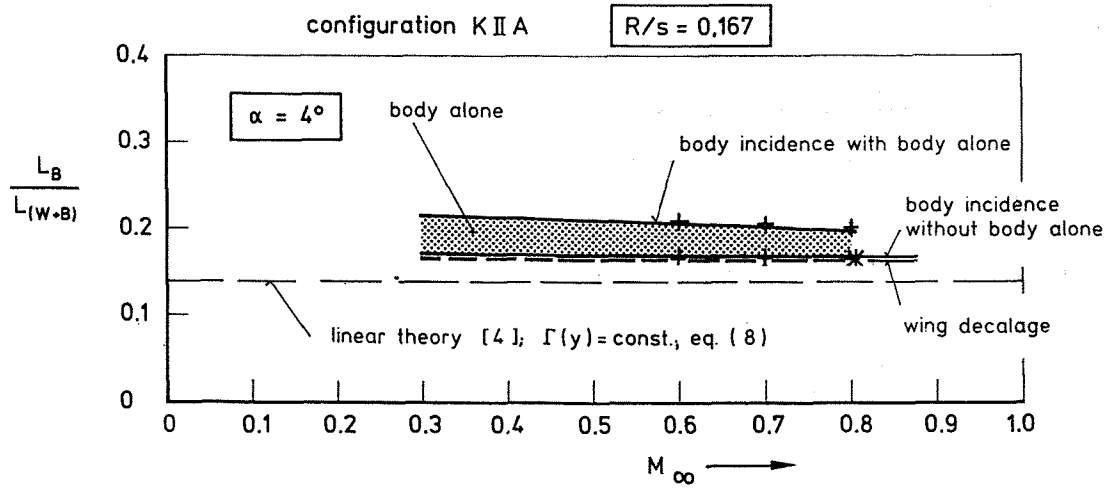

	without wing boundary layer	with wing boundary layer
body incidence (α = 4°, ε = 0°)	———	+
wing decalage (α = 0°, ε = 4°)	— — — —	×

Fig. 19 Lift ratio $L_B/L_{(W+B)}$ of the principle model in dependence of Mach number

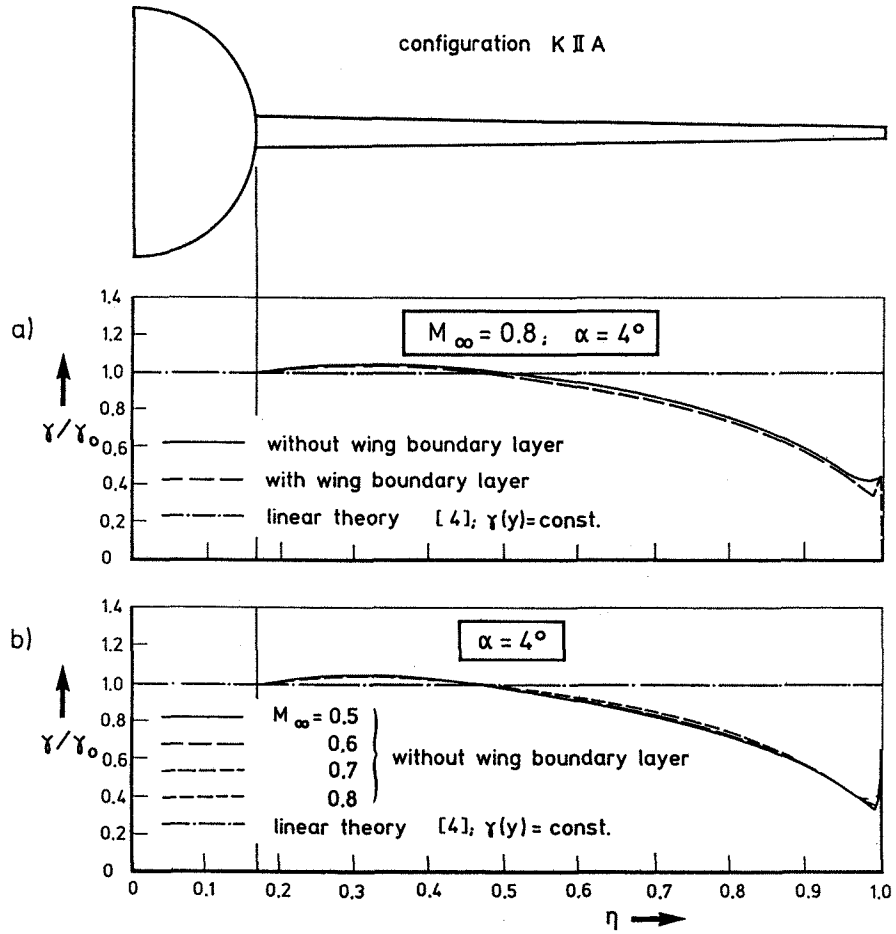

Fig. 20 Deviation of spanwise distribution of wing circulation from the constant value (configuration KIIA)

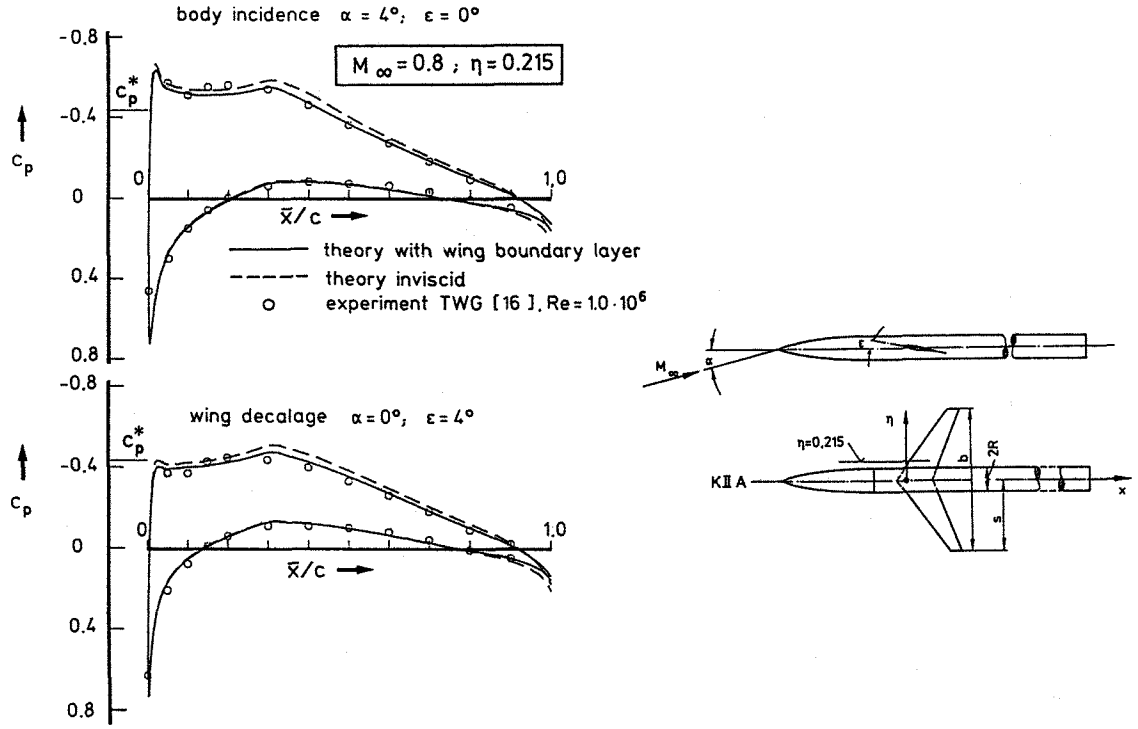

Fig. 21 Comparison with measurements (TWG) [16]: Wing pressure distributions: Body with incidence and wing decalage